

## Article

# Mechanochemical Induced Structure Transformations in Lithium Titanates: A Detailed PXRD and $^6\text{Li}$ MAS NMR Study

Dennis Becker, Robert Haberkorn and Guido Kickelbick \*

Saarland University, Inorganic Solid State Chemistry, Campus, Building C 41, 66123 Saarbrücken, Germany

\* Correspondence: guido.kickelbick@uni-saarland.de; Tel.: +49-681-302-70651

**Abstract:** Lithium titanates are used in various applications, such as anode materials for lithium intercalation ( $\text{Li}_4\text{Ti}_5\text{O}_{12}$ ) or breeding materials in fusion reactors ( $\text{Li}_2\text{TiO}_3$ ). Here, we report the formation of nano-crystalline lithium titanates by a mechanochemical approach and present a deeper insight into their structural characteristics by PXRD and solid-state NMR spectroscopy. The compounds were synthesized in a high energy planetary ball mill with varying milling parameters and different grinding tools. NaCl type  $\text{Li}_2\text{TiO}_3$  ( $\alpha\text{-Li}_2\text{TiO}_3$ ) was formed by dry milling of lithium hydroxide with titania (rutile or anatase) and by a milling induced structure transformation of monoclinic  $\beta\text{-Li}_2\text{TiO}_3$  or spinel type  $\text{Li}_4\text{Ti}_5\text{O}_{12}$ . Heating of mechanochemical prepared  $\alpha\text{-Li}_2\text{TiO}_3$  induces a phase transformation to the monoclinic phase similar to hydrothermal reaction products, but a higher thermal stability was observed for the mechanochemical formed product. Microstructure and crystallographic structure were characterized by PXRD via Rietveld analysis. Detailed phase analysis shows the formation of the cubic phase from the various educts. A set of two lattice parameters for  $\alpha\text{-Li}_2\text{TiO}_3$  was refined, depending on the presence of  $\text{OH}^-$  during the milling process. An average crystallite size of less than 15 nm was observed for the mechanochemical generated products. The local Li environment detected by  $^6\text{Li}$  SPE MAS NMR revealed Li defects in the form of tetrahedral instead of octahedral site occupation. Subsequent adjustment of the structural model for Rietveld refinement leads to better fits, supporting this interpretation.

**Keywords:** lithium titanium oxide, mechanochemistry, high energy ball milling, X-ray diffraction, Rietveld refinement,  $^6\text{Li}$  SPE MAS NMR, impedance spectroscopy

## 1. Introduction

High energy ball milling (*hebm*) is a versatile tool in the synthesis of metal oxides [1]. Beside the formation of oxide phases that can also be produced in other solid-state reactions, such as high temperature or hydrothermal reactions, it is possible to obtain nanocrystalline high-temperature or high-pressure phases that are not accessible with traditional synthetic techniques. Examples are the formation of a high-pressure polymorph of  $\text{TiO}_2$  starting from anatase or the formation of a  $(\text{Zr}_{1-x}\text{Ti}_x)\text{O}_2$  solid solution [2,3]. The milling process can also be used for a solvent free surface functionalization of nanocrystallites due to the formation of reactive surfaces during the milling process [4]. Additionally, milling generates defects in the form of oxygen vacancies in anatase, as shown by impedance spectroscopy measurements [5].

$\text{Li}_2\text{TiO}_3$  represents an interesting system for high energy ball milling because of the three known polymorphs that might be converted under the milling conditions depending on the energy impact. The monoclinic low temperature modification  $\beta\text{-Li}_2\text{TiO}_3$  (Figure 1a) with space group  $C2/c$  has a layered structure with three different lithium sites and two different titanium sites and is isostructural to  $\text{Li}_2\text{SnO}_3$  [6–9]. The cubic high temperature modification  $\gamma\text{-Li}_2\text{TiO}_3$  (Figure 1b) with space group  $Fm\text{-}3m$  consists of a NaCl type structure with statistical distribution of  $\text{Li}^+$  and  $\text{Ti}^{4+}$  on the  $4a$  site and  $Z = 4/3$  formula units per unit cell ( $\text{Li}_{2.66}\text{Ti}_{1.33}\text{O}_4$ ) [7–9]. The  $\beta$  polymorph undergoes a reversible

transformation to the  $\gamma$  polymorph at approximately 1150 °C [7,10]. A metastable cubic low temperature form with space group  $Fm-3m$  is obtained by hydrothermal reactions from LiOH and TiO<sub>2</sub> in water and is denoted as  $\alpha$ -Li<sub>2</sub>TiO<sub>3</sub> [7,11–13]. An irreversible phase transformation from hydrothermally formed  $\alpha$ -Li<sub>2</sub>TiO<sub>3</sub> to  $\beta$ -Li<sub>2</sub>TiO<sub>3</sub> occurs after heating above 300 °C [13–15].

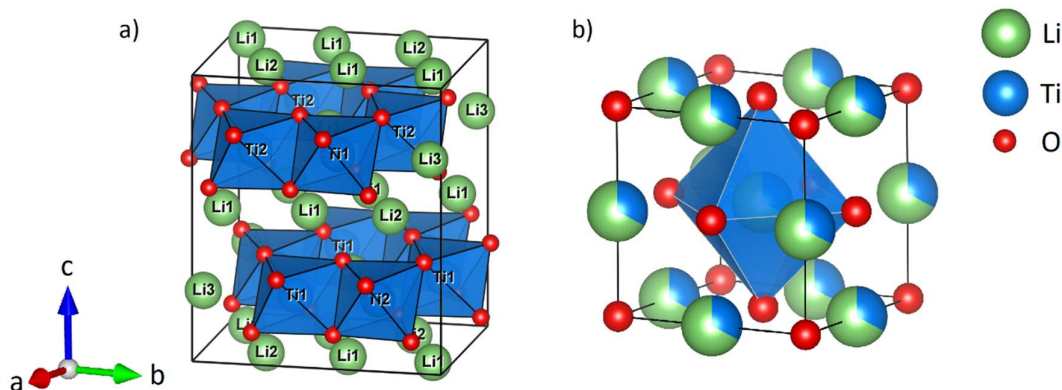


**Figure 1:** Unit cell of monoclinic  $\beta$ -Li<sub>2</sub>TiO<sub>3</sub> (left) and cubic  $\alpha/\gamma$ -Li<sub>2</sub>TiO<sub>3</sub> (right). The green spheres represent lithium, blue titanium and red oxygen. Only polyhedra around titanium (left) or a single octahedra (right) are shown, to emphasize the structural features.

Ball milling of monoclinic  $\beta$ -Li<sub>2</sub>TiO<sub>3</sub> enhances the long-range ion transport, while also inducing a partial transformation to the cubic  $\alpha$  polymorph and amorphization, but neither quantitative conversion nor details of the structural properties or phase compositions after milling were reported yet [16]. The  $\alpha$  polymorph may also be obtained by milling of NaOH, LiCl and TiO<sub>2</sub>, but subsequent washing to remove NaCl is necessary and no structural characterization of the product is given [17]. For Li<sub>4</sub>Ti<sub>5</sub>O<sub>12</sub>, a well-known Li-ion battery anode material, an increase in ion conductivity is reported after milling, but no structure transformation or structural changes by milling were reported in literature yet [18].

The goal of our study was the investigation of mechanochemical induced processes in lithium titanates and the systematic study of process parameters such as milling tools, milling times and milling speed *via* detailed PXRD Rietveld refinement and <sup>6</sup>Li SPE MAS NMR experiments. The mechanochemical induced synthesis of cubic  $\alpha$ -Li<sub>2</sub>TiO<sub>3</sub> from the simple educts LiOH and TiO<sub>2</sub> is reported for the first time and its thermal stability is explored by PXRD. Furthermore, the mechanochemical induced phase transformation of  $\beta$ - to  $\alpha$ -Li<sub>2</sub>TiO<sub>3</sub> is examined by PXRD and additionally by <sup>6</sup>Li NMR experiments, revealing occupation of tetrahedral sites by lithium. Subsequent modification of the structural model for  $\alpha$ -Li<sub>2</sub>TiO<sub>3</sub> improves the Rietveld refinement. Lastly, PXRD and <sup>6</sup>Li NMR experiments reveal a strong structural influence on spinel Li<sub>4</sub>Ti<sub>5</sub>O<sub>12</sub> by mechanochemical treatment.

## 2. Results and Discussion

### 2.1 Mechanochemical formation of $\alpha$ -Li<sub>2</sub>TiO<sub>3</sub> from LiOH and TiO<sub>2</sub>

High energy ball milling of LiOH with rutile or anatase as titania precursors in yttrium stabilized zirconia (ZrO<sub>2</sub>) and tungsten carbide/cobalt hard metal (WC) tools lead to the formation of new reflections in the X-ray diffractogram which may be indexed by a cubic unit cell, as already in a previous study [19]. The new reflections could be assigned to either LiTiO<sub>2</sub> or Li<sub>2</sub>TiO<sub>3</sub> with NaCl type structure (SG  $Fm-3m$ ) and a refined lattice parameter  $a$  varying between 4.15 and 4.16 Å, depending on the reaction conditions. While both compounds have the same structure type, a quantitative reduction of Ti<sup>4+</sup> to Ti<sup>3+</sup> is required to form LiTiO<sub>2</sub>. This is unlikely under the given conditions, since a reducing agent or oxygen release would be necessary. However, the appearance of very small portions of Ti<sup>3+</sup> in TiO<sub>2</sub> has been described as a result of defect formation by mechanochemical

methods [20]. The mechanochemical formation of  $\text{LiTiO}_2$  has been described before by milling of  $\text{Li}_2\text{O}$ ,  $\text{TiO}_2$  and  $\text{Ti}$ , with larger impurities of elemental iron from abrasion of the steel milling tools [21]. Furthermore,  $\text{LiTiO}_2$  is black in color [22], while the products of our process are white if  $\text{ZrO}_2$  tools are used or gray if WC tools are used. The grey color is based upon abrasion from the WC tools [23]. Hence, the composition of the milling products corresponds to a composition close to  $\text{Li}_2\text{TiO}_3$  with a mean Ti oxidation state of nearly IV. Due to the additional anatase to high pressure phase transformation [2], milling products of  $\text{LiOH}$  and anatase show a complex phase composition. The Rietveld refinement of the milling product from  $\text{ZrO}_2$  tools after 6 h of milling at 600 rpm is shown as an example in the supporting information (Figure S11). The reflections of the high-pressure polymorph  $\text{TiO}_2$ -II overlap with the reflections of anatase and  $\alpha\text{-Li}_2\text{TiO}_3$ . Additionally, milling with anatase as the titania precursor leads to a smaller portion of cubic phase after the same milling conditions.

Based on the reported results we decided to only discuss the rutile ball milling more closely in the following sections. PXRD measurements of  $\text{LiOH}$ , rutile and the milling products with different parameters are shown in Figure 2. Decrease of the  $\text{TiO}_2$  main reflection and rise of new  $\alpha\text{-Li}_2\text{TiO}_3$  reflections are marked by yellow rectangles. Formation of  $\text{Li}_2\text{CO}_3$  (marked by triangles) is caused by unreacted amorphous  $\text{LiOH}$  which forms crystalline  $\text{Li}_2\text{CO}_3$  on contact with air, allowing for a quantification by Rietveld refinement.

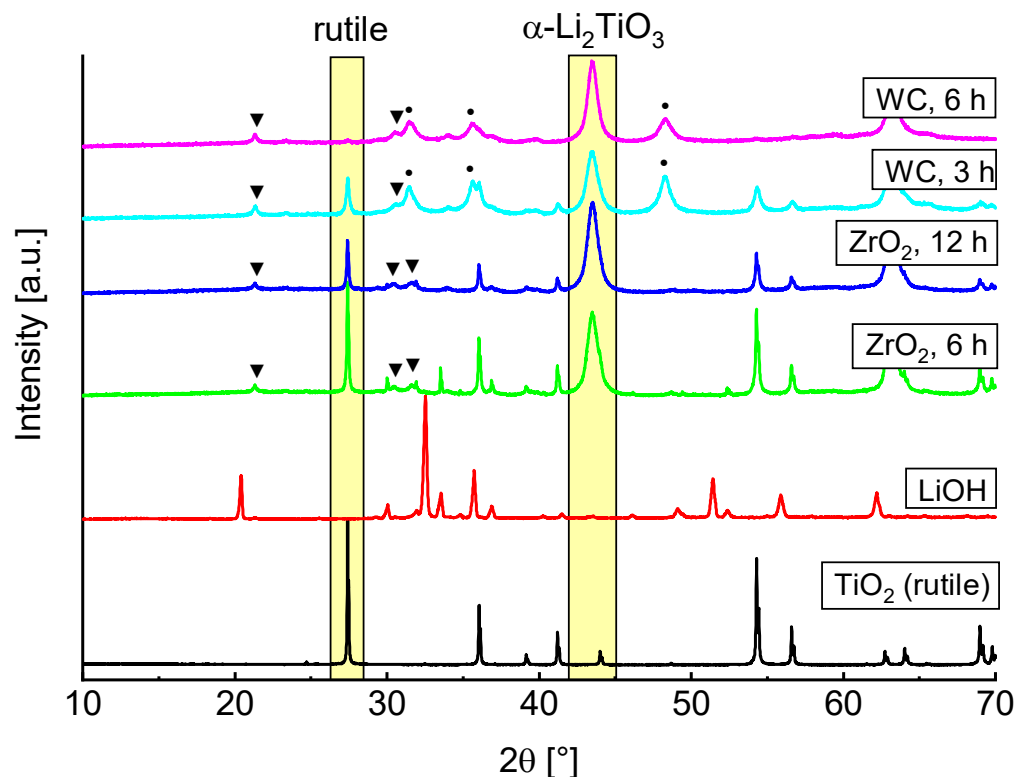


**Figure 2:** PXRD measurements of  $\text{LiOH}$  and rutile after different milling conditions. Excess  $\text{LiOH}$  forms  $\text{Li}_2\text{CO}_3$  after the milling process (triangles). WC reflections (circles) arise due to abrasion of the tools.

A faster formation of  $\alpha\text{-Li}_2\text{TiO}_3$  can be observed by use of WC milling tools. Rietveld refinements indicate an introduction of 2 to 4% crystalline WC from abrasion of the tools (marked by circles). After a milling time of 6 h no rutile reflections are any more visible, while these are still present after 12 h if  $\text{ZrO}_2$  tools are used. This is most likely due to the different hardness of the milling tools and the resulting variations in impact energies. There are already reports in literature which indicate that the milling tools can have a large influence on the formation of different phases [3,24].

Only results obtained by using WC tools are discussed more closely in the following, since they show a more efficient conversion to cubic  $\text{Li}_2\text{TiO}_3$ . Depending on the milling parameters, the refined structural parameters of the PXRD measurements are slightly different. The lattice parameter  $a$  varies and the crystallite size is in the range of 10 to 15 nm. Since  $\text{OH}^-$  anions are readily available by using  $\text{LiOH}$  in the mechanochemical synthesis, substitution of  $\text{O}^{2-}$  by  $\text{OH}^-$  may be the case to some extent, resulting in a variation of the lattice parameter (4.15–4.16 Å) depending on the degree of substitution. Because only traces of  $\text{H}_2\text{O}$  were found during TG-IR investigation (supporting information Figures SI4 and SI5) only a small amount of  $\text{OH}^-$  may be assumed but different  $\text{OH}^-$  contents caused by varying conditions of synthesis account for the different lattice parameters of the as prepared products.

Higher amounts of cubic  $\text{Li}_2\text{TiO}_3$  were only obtained after long milling times or high milling speeds (Figure 3). The cubic phase formed slowly at lower rotational speeds (400 rpm) and even after 24 h a portion of 50% was not exceeded. At high milling speeds (600 rpm) a portion larger than 50% was already achieved after milling for only three hours.

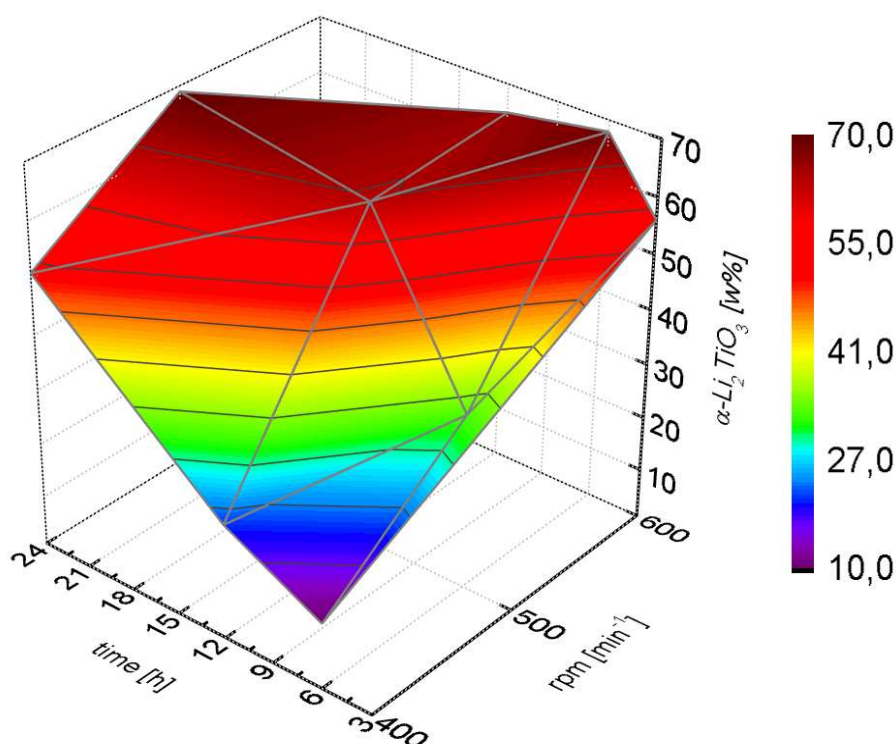


**Figure 3:** Weight portions (from Rietveld refinement) of  $\alpha\text{-Li}_2\text{TiO}_3$  after milling of  $\text{LiOH}$  and rutile in WC tools with different parameters.

The percentage of  $\alpha\text{-Li}_2\text{TiO}_3$  after milling at 600 rpm for 6 h amounts to 68%, as analyzed by Rietveld refinement (Figure 4) neglecting possibly existing amorphous matter. Since  $\text{Li}_2\text{CO}_3$  is still present after complete conversion of  $\text{TiO}_2$  and an increased baseline intensity is visible, a portion of amorphous material may be assumed. Handling of the milling product in a glovebox with subsequent measurement in an airtight dome sample holder (Rietveld refinement in supporting information figure SI2) reveals no crystalline phase of  $\text{LiOH}$  nor  $\text{Li}_2\text{CO}_3$ , therefore  $\text{Li}_2\text{CO}_3$  is formed after the milling process from the amorphous material by exposure to air. Measurements with an internal standard (50% of  $\alpha\text{-Al}_2\text{O}_3$ ) led to the identification of approximately 35% amorphous content, which may contain missing amounts of  $\text{TiO}_2$ .

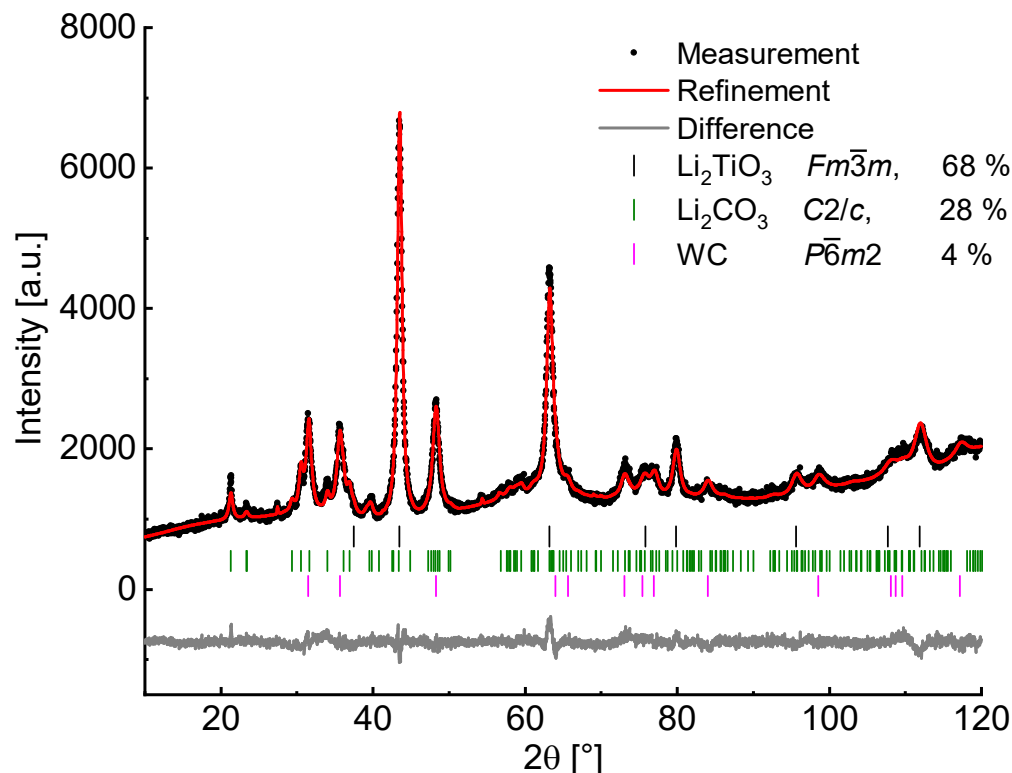


**Figure 4:** Rietveld plot of the milling product from LiOH and rutile (WC tools, 600 rpm, 6h).  $\text{Li}_2\text{TiO}_3$  in SG  $Fm\bar{3}m$  with  $a = 4.1588(2) \text{ \AA}$ ,  $V = 71.93(1) \text{ \AA}^3$ , number of reflections = 8 and  $R_{\text{Bragg}} = 1.17\%$ . Refinement parameters: number of independent parameters = 40,  $R_{\text{wp}} = 3.44\%$ ,  $R_{\text{exp}} = 2.60\%$ ,  $GOF = 1.32$ . For more detailed refinement parameters see supporting information table SI1.

If the amorphous content is assumed to contain the starting composition, the total formula may be written as  $\text{Li}_{2-4x}\text{Ti}_{1+x}\text{O}_3$  to consider a non-stoichiometry. A formula of  $\text{Li}_{1.4}\text{Ti}_{1.15}\text{O}_3$  ( $x = 0.15$ ) is necessary to stay in the range of the starting composition with a Li to Ti ratio of 2:1. A constrained refinement of the Li and Ti occupancy on the  $4a$  site of  $\alpha\text{-Li}_2\text{TiO}_3$  suggests a lithium deficiency, too. However, to preserve electric neutrality one titanium substitutes four lithium atoms resulting in a small electronic contrast and accordingly, these refinements rather represent a general tendency and no absolute values. Since  $\text{Li}_2\text{CO}_3$  crystallized only after the reaction, the remaining amorphous content may be assumed to be only or mainly  $\text{TiO}_2$  in which case a nearly stoichiometric compound with the formula  $\text{Li}_2\text{TiO}_3$  would be obtained. Thermogravimetric analysis reveals a mass loss of 16.2% (supporting information Figure SI4) upon heating to 1000 °C. IR coupling of the gas flow shows primarily characteristic bands of carbon dioxide besides traces of  $\text{H}_2\text{O}$  (supporting information Figure SI5), indicating crystalline  $\text{Li}_2\text{CO}_3$  as main fraction responsible for the mass loss. Therefore, the amorphous background is assumed to be primarily  $\text{TiO}_2$ .

SEM images (supporting information, Figure SI3) indicate that large agglomerates with seemingly granular surface were formed in the milling process. The primary grains of the agglomerates that form the surface are visible. The grain size of the primary grains is in the range of 20 nm and is of the same order as the refined crystallite sizes.

## 2.2 Thermal transformation of $\alpha\text{-Li}_2\text{TiO}_3$ to $\beta\text{-Li}_2\text{TiO}_3$

The thermal stability of mechanochemical formed  $\alpha\text{-Li}_2\text{TiO}_3$  (milling of LiOH and rutile in WC tools at 600 rpm for 6 h) was investigated by successive heating in 100 K steps for 1 h respectively



and subsequent PXRD measurement at ambient conditions after each step (Figure 5). Between 300 and 500 °C, the formation of a broad reflection in the range around 20° 2 $\theta$  indicates a short-range ordering phenomenon. Since the range in which the reflection is formed coincides with the position of the 002-reflection (18.5°) of  $\beta$ -Li<sub>2</sub>TiO<sub>3</sub>, the broad reflection is probably caused by the nucleation of the monoclinic phase. Sharp reflections of  $\beta$ -Li<sub>2</sub>TiO<sub>3</sub> become evident between 500 and 600 °C. The transformation is completed at temperatures over 700 °C. Compared to the hydrothermal synthesis of  $\alpha$ -Li<sub>2</sub>TiO<sub>3</sub>, sharp reflections of  $\beta$ -Li<sub>2</sub>TiO<sub>3</sub> are visible at 420 °C and the transformation is nearly complete at 500 °C with only minor amounts of the  $\alpha$ -phase visible (estimated at 12%) [14].

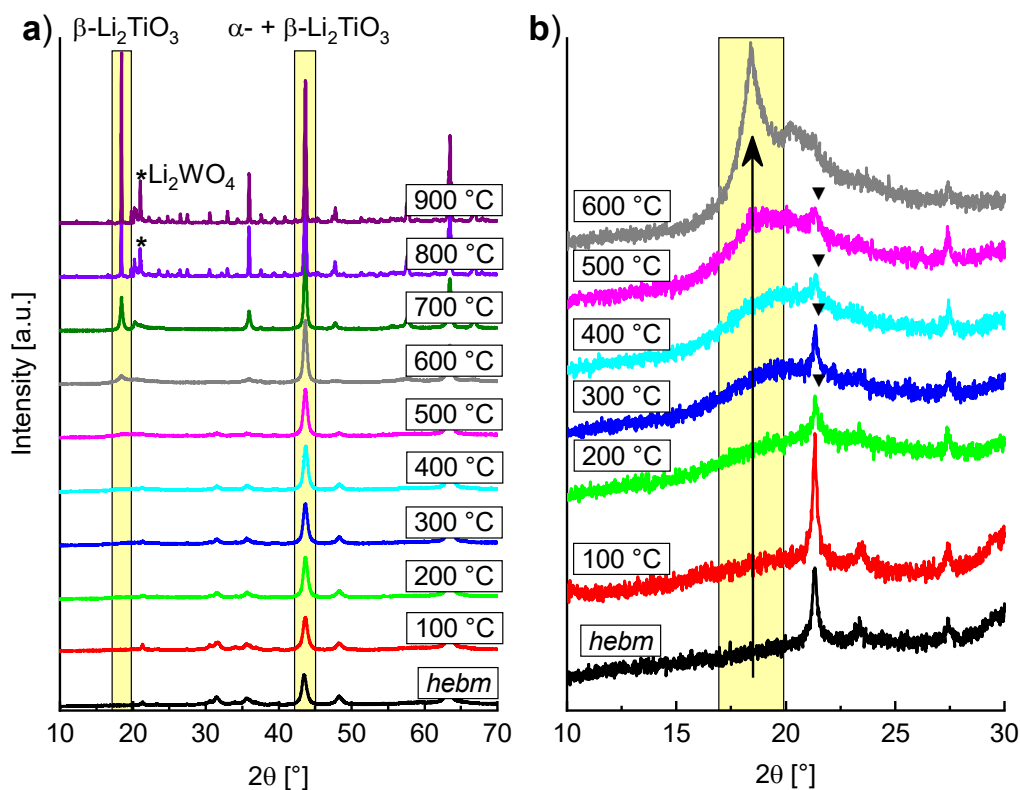


**Figure 5:** PXRD measurements of hebm Li<sub>2</sub>TiO<sub>3</sub> after heating to different temperatures for 1 h. a) Main reflections of  $\beta$ - and  $\alpha$ -Li<sub>2</sub>TiO<sub>3</sub> are highlighted. b) The arrow indicates the deployment of the (002) reflection of  $\beta$ -Li<sub>2</sub>TiO<sub>3</sub> between 500 and 600 °C. Triangles indicate the main reflection of Li<sub>2</sub>CO<sub>3</sub>.

The lattice parameter  $a$  of  $\alpha$ -Li<sub>2</sub>TiO<sub>3</sub> changes from 4.1588(2) to 4.1435(1) Å after heating to 200 °C for 1 h. This may be a consequence of the previously mentioned hypothetical OH<sup>-</sup> contents in the lattice of an as prepared  $\alpha$ -Li<sub>2</sub>TiO<sub>3</sub>. Heating induces a transformation of OH<sup>-</sup> to O<sup>2-</sup> and H<sub>2</sub>O, leaving the cubic phase with a smaller lattice parameter. Additionally, a high phase portion of  $\alpha$ -Li<sub>2</sub>TiO<sub>3</sub> has been obtained under these mild conditions, with only 7% Li<sub>2</sub>CO<sub>3</sub> remaining and without affecting crystallite size of the cubic phase (Rietveld refinement shown in supporting information, Figure SI6).

In the temperature range between 300 °C and 600 °C a single fraction of  $\beta$ -Li<sub>2</sub>TiO<sub>3</sub> was used in the refinements to estimate the proportion of cubic and monoclinic Li<sub>2</sub>TiO<sub>3</sub>. Starting with a temperature of 600 °C a three-fraction model for  $\beta$ -Li<sub>2</sub>TiO<sub>3</sub> was used (described under 3.4 *Structural model for  $\beta$ -Li<sub>2</sub>TiO<sub>3</sub> in Rietveld refinement*). Increasing amounts of 30 to 90% monoclinic fraction were refined in the temperature range between 300 and 700 °C, while the amount of  $\alpha$ -Li<sub>2</sub>TiO<sub>3</sub> was decreasing. However, up to 500 °C the intensities of the cubic reflections are hardly affected. This either indicates that the monoclinic ordering arises from byproducts without affecting the cubic structure, or that the ordering takes place continuously. The refined phase portions of  $\alpha$ -Li<sub>2</sub>TiO<sub>3</sub> (cubic) Li<sub>2</sub>CO<sub>3</sub> and  $\beta$ -Li<sub>2</sub>TiO<sub>3</sub> (monoclinic) are depicted in Figure 6 with the corresponding calcination temperature.

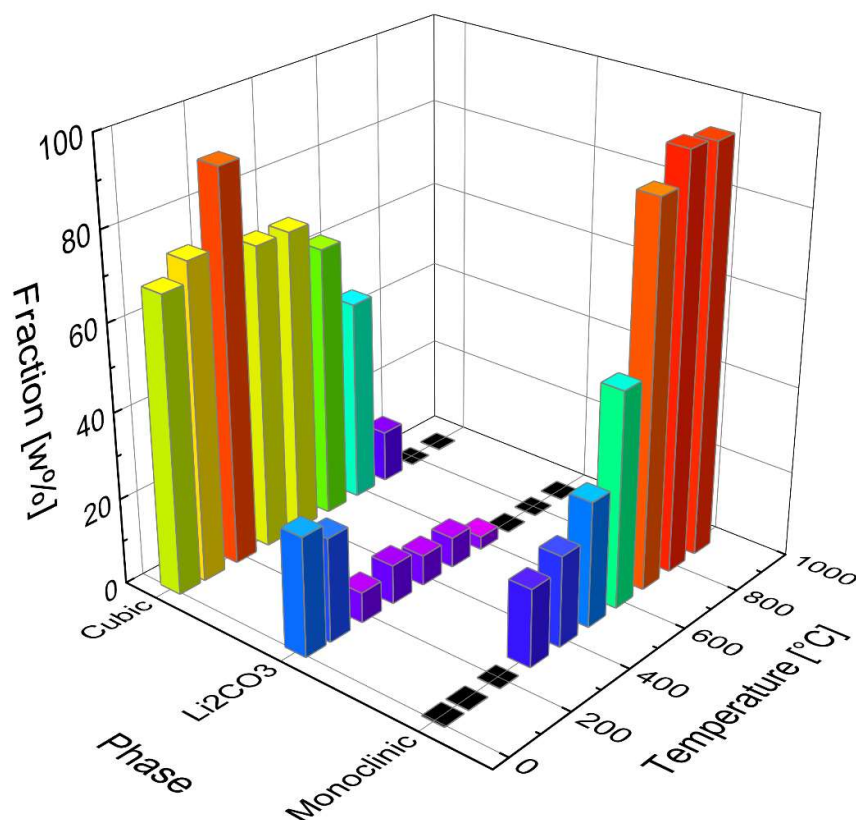


**Figure 6:** Graphical representation of the refined phase portions of  $\alpha$ -Li<sub>2</sub>TiO<sub>3</sub> (cubic) Li<sub>2</sub>CO<sub>3</sub> and  $\beta$ -Li<sub>2</sub>TiO<sub>3</sub> (monoclinic) and the corresponding calcination temperature.

Thermogravimetric analysis (supporting information, Figure SI4) between 25 and 1000 °C shows a mass loss up to the temperature range of 575 to 600 °C (attributed to Li<sub>2</sub>CO<sub>3</sub>). An exothermic signal arises in the calculated DTA curve, which correlates to the complete crystallization of  $\beta$ -Li<sub>2</sub>TiO<sub>3</sub> as observed in the PXRD measurements. At 600 °C a composition with equal amounts of  $\alpha$ - and  $\beta$ -Li<sub>2</sub>TiO<sub>3</sub> was refined. Fitting with only the monoclinic phase lead to an insufficient refinement ( $GOF=4.39$ ) while inclusion of the cubic phase results in a greatly improved description ( $GOF=1.42$ ). At 700 °C an abrupt increase to > 90%  $\beta$ -Li<sub>2</sub>TiO<sub>3</sub> occurs, with only minor amounts of the cubic phase remaining. Fitting with only the monoclinic structure results in a similar description ( $GOF=2.09$ ) as by using both structures ( $GOF=1.93$ ). Though the improvement of the description is small, this may still be accounted to remaining portions of the cubic phase. This leads to an overall interpretation that an ordering phenomenon takes place in the cubic phase at lower temperatures with a discrete structure change between 600 and 700 °C.

### 2.3 Mechanochemical induced phase transformation of $\beta$ -Li<sub>2</sub>TiO<sub>3</sub> and spinel Li<sub>4</sub>Ti<sub>5</sub>O<sub>12</sub> to $\alpha$ -Li<sub>2</sub>TiO<sub>3</sub>

The ball milling induced phase transformation from  $\beta$ - to  $\alpha$ -Li<sub>2</sub>TiO<sub>3</sub> has already been mentioned by Brandstätter et al. [16], but no further investigation in terms of a quantitative conversion was conducted. In Figure 7, PXRD measurements of  $\beta$ -Li<sub>2</sub>TiO<sub>3</sub> before and after milling with a) ZrO<sub>2</sub> tools and b) WC tools at different parameters are shown. In both cases a) and b) a decrease of the  $\beta$ -Li<sub>2</sub>TiO<sub>3</sub> main reflection can be seen. Milling with ZrO<sub>2</sub> tools at 600 rpm for 6 h leads to portions of 48%  $\alpha$ -Li<sub>2</sub>TiO<sub>3</sub>, 25%  $\beta$ -Li<sub>2</sub>TiO<sub>3</sub> and 28% Li<sub>2</sub>CO<sub>3</sub>. Prolonged milling leads to a further increase in intensity of Li<sub>2</sub>CO<sub>3</sub> reflections. In contrast, the ball milling induced phase transformation is already detectable after milling for 10 min in WC tools. A portion of ca. 30%  $\alpha$ -Li<sub>2</sub>TiO<sub>3</sub> can be fitted, with

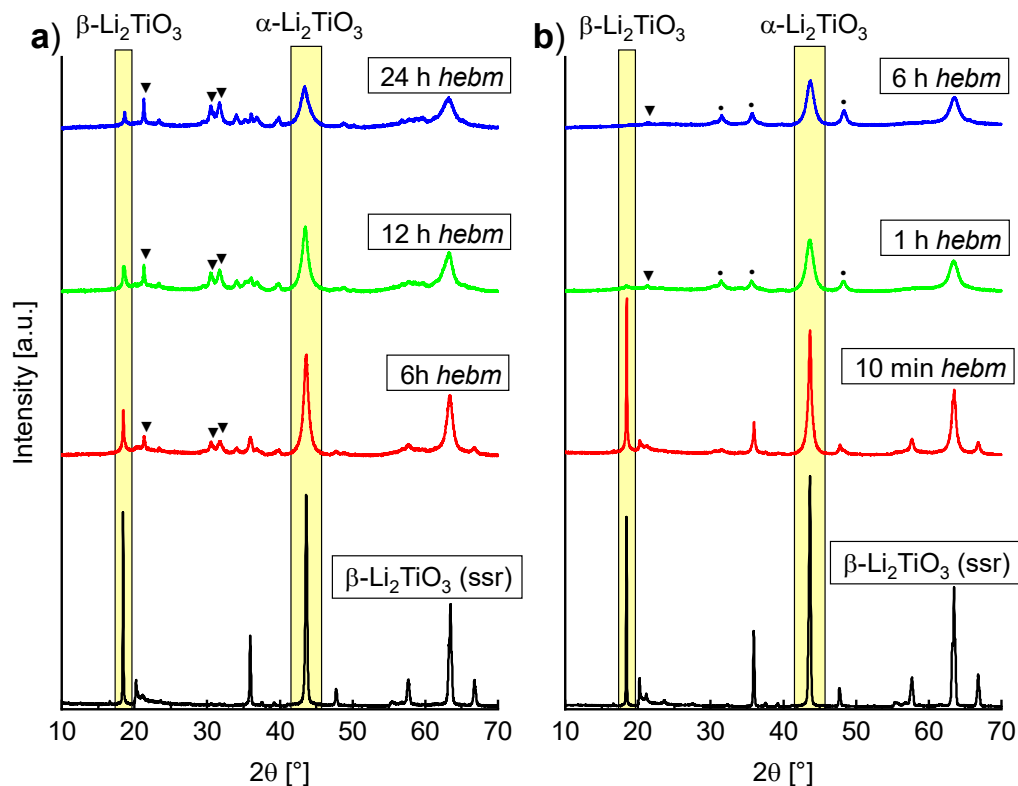


**Figure 7:** PXRD measurements of  $\beta$ - $\text{Li}_2\text{TiO}_3$  after milling in a)  $\text{ZrO}_2$  and b) WC tools at 600 rpm after different grinding times. Triangles indicate  $\text{Li}_2\text{CO}_3$ , circles indicate WC.

small amounts of  $\text{Li}_2\text{CO}_3$  (< 10%). Even after milling for 1 h, only marginal amounts of ca. 5%  $\beta$ - $\text{Li}_2\text{TiO}_3$  remained. Milling with WC tools leads to complete disappearance of  $\beta$ - $\text{Li}_2\text{TiO}_3$  reflections after 6 h. Portions of 89%  $\alpha$ - $\text{Li}_2\text{TiO}_3$ , 8%  $\text{Li}_2\text{CO}_3$  and 3% WC have been refined (Rietveld refinement in supporting information, Figure SI7). Similar to the mechanochemical synthesis from  $\text{LiOH}$  and rutile, an increase in baseline intensity suggests the formation of amorphous material. Refinement of  $\beta$ - $\text{Li}_2\text{TiO}_3$  (milling in WC tools for 6 h) with an internal standard (50% of  $\alpha$ - $\text{Al}_2\text{O}_3$ ) suggests a portion of 27% amorphous background. In comparison to the mechanochemical synthesis from  $\text{LiOH}$  and rutile in WC tools, a smaller lattice parameter  $a = 4.1463(2) \text{ \AA}$  is refined for  $\alpha$ - $\text{Li}_2\text{TiO}_3$  if  $\beta$ - $\text{Li}_2\text{TiO}_3$  is used as educt. This may also be a consequence of the previously mentioned hypothetical  $\text{OH}^-$  contents in the lattice. Since no  $\text{OH}^-$  is available in the mechanochemical induced phase transformation of  $\beta$ - to  $\alpha$ - $\text{Li}_2\text{TiO}_3$  a lattice parameter similar to the one of  $\alpha$ - $\text{Li}_2\text{TiO}_3$  after heating to  $200^\circ\text{C}$  is refined.

Formation of  $\alpha$ - $\text{Li}_2\text{TiO}_3$  is also observed by milling of  $\text{Li}_4\text{Ti}_5\text{O}_{12}$  with spinel type structure. PXRD measurements of  $\text{Li}_4\text{Ti}_5\text{O}_{12}$  before and after milling in WC tools at 400 rpm are shown in Figure 8a. After a milling time of 1 h a slight asymmetric broadening of the (400) reflection is visible, while the (111) reflection is not as strongly affected and shows little asymmetry. This is caused by the formation of  $\alpha$ - $\text{Li}_2\text{TiO}_3$  whose reflections overlap with the spinel reflections. In Figure 8b the Bragg intensities of the spinel (400) and the  $\alpha$ - $\text{Li}_2\text{TiO}_3$  (200) reflection are shown with the resulting Rietveld fit. The (111) reflection of the spinel phase vanishes completely after a milling time of 6 h. Though a phase with cubic structure is formed, the intensities are very low and additional unidentified reflections are visible. Even after these mild milling conditions, the structure of the spinel phase is strongly altered, which may have large impact on the use of mechanochemically treated  $\text{Li}_4\text{Ti}_5\text{O}_{12}$  as anode material in battery applications. It has already been established by impedance spectroscopy that milling of  $\text{Li}_4\text{Ti}_5\text{O}_{12}$  leads to an increase in conductivity [18]. This may be due to this partial structure transformation of spinel  $\text{Li}_4\text{Ti}_5\text{O}_{12}$  to  $\alpha$ - $\text{Li}_2\text{TiO}_3$ .



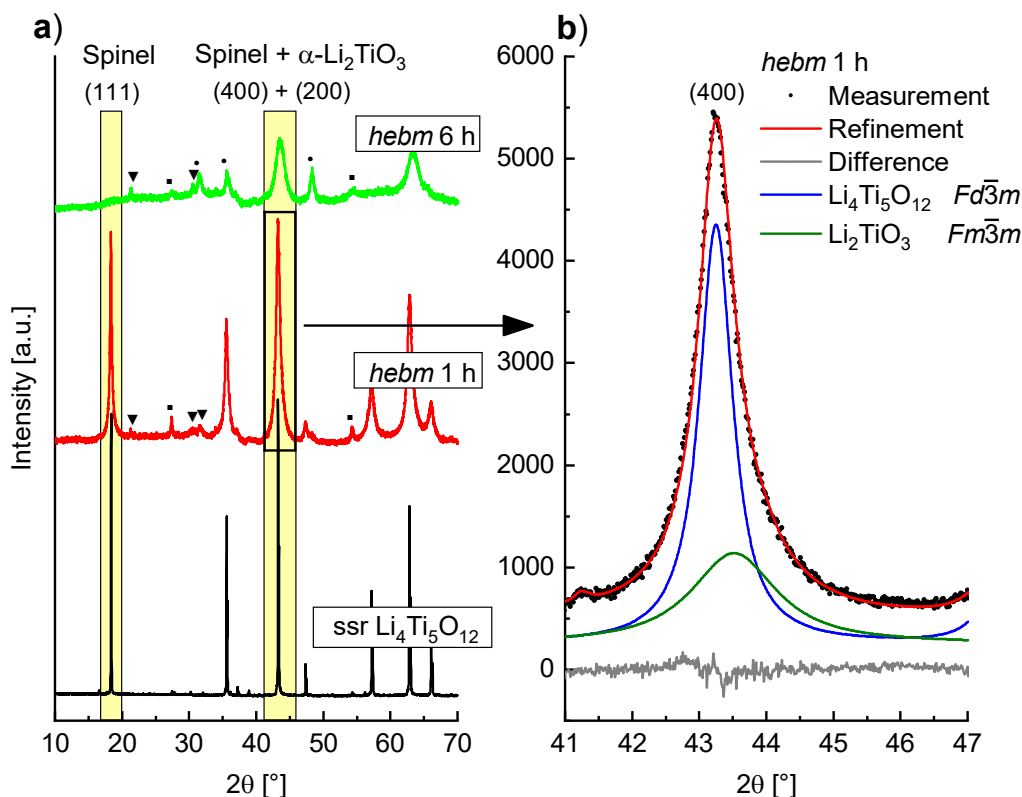


**Figure 8:** a) PXRD of spinel  $\text{Li}_4\text{Ti}_5\text{O}_{12}$  before and after milling in WC tools at 400 rpm for 1 h and 6 h. Data of  $\text{Li}_4\text{Ti}_5\text{O}_{12}$  were scaled by a factor of 0.5. Triangles indicate  $\text{Li}_2\text{CO}_3$ , squares indicate rutile and circles indicate WC reflections. b) Enhanced section of the Rietveld plot after milling for 1 h, with fitted portions of spinel (blue) and NaCl type structure (green).

#### 2.4 $^6\text{Li}$ SPE MAS NMR

$^6\text{Li}$  SPE MAS NMR experiments reveal additional insight into the milling induced structure transformation. To illustrate the following interpretations, the unit cell of spinel  $\text{Li}_4\text{Ti}_5\text{O}_{12}$  is shown in Figure 9. (The unit cell of monoclinic  $\beta\text{-Li}_2\text{TiO}_3$  is shown in Figure 1).

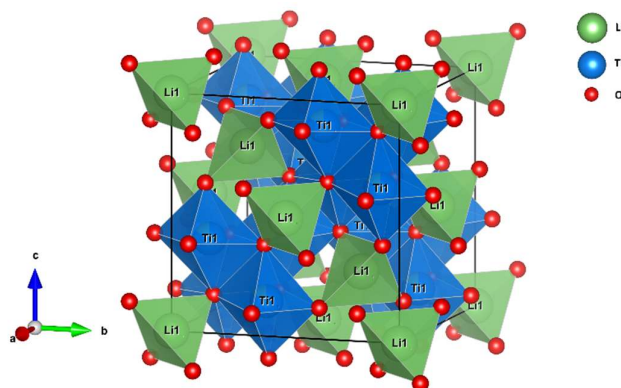


**Figure 9:** Unit cell of spinel  $\text{Li}_4\text{Ti}_5\text{O}_{12}$ . The green spheres represent lithium, blue titanium and red oxygen. The Ti1 position inside the octahedra are occupied by 0.833 Ti and 0.167 Li.

PXRD refinements of 900 °C sintered  $\beta\text{-Li}_2\text{TiO}_3$  with constrained lithium site occupancy factors (total Li content is 2.0 Li per formula unit) show a full occupation of the 8f and 4d site (Li1 and Li2),

while the  $4e$  lithium site (Li3) and the two titanium  $4e$  sites (Ti1 and Ti2) show a mixed occupation with 0.6 Li on the Li3 site, 0.3 Li on the Ti1 site and 0.1 Li on the Ti2 site. To obtain a sample with low Li3/Ti1/Ti2 anti site mixing, several sintering steps at 1100 °C were necessary. A mixing of 0.1 Li on the Ti1 site and 0.1 Li on the Ti2 site remained.

The  $^6\text{Li}$  NMR spectrum of 1100 °C sintered  $\beta\text{-Li}_2\text{TiO}_3$  is shown in Figure 10a where three signals are visible. Fitting of the line profile was performed with 3 independent Voigt functions, resulting in shifts of  $\delta = 1.30, 0.80$  and  $0.23$  ppm. The peak at  $0.80$  ppm is attributed to lithium on the  $4e$  site (Li3) in the  $\text{LiTi}_2$  layer, the peak at  $0.23$  ppm originates from the two magnetically equivalent lithium sites  $8f$  (Li1) and  $4d$  (Li2) in the  $\text{Li}_2$  layer [25,26]. The signals are consistent with values reported in the literature if an offset of ca.  $-1$  ppm is considered due to the referencing against solid LiCl [27]. The shift of the third signal matches a tetrahedral coordination of lithium [25]. In Figure 10b the  $^6\text{Li}$  spectrum of spinel  $\text{Li}_4\text{Ti}_5\text{O}_{12}$  is shown.  $\text{Li}_4\text{Ti}_5\text{O}_{12}$  may also be written as  $(\text{Li})[\text{Li}_{0.33}\text{Ti}_{1.66}]\text{O}_4$  to illustrate the occupation of 1 Li on the tetrahedral and  $\frac{1}{3}$  Li on the octahedral position. According to literature the peak at  $1.32$  ppm is attributed to tetrahedrally coordinated lithium on the  $8a$  site and the smaller peak at  $0.96$  ppm to octahedrally coordinated lithium on the  $16d$  site [28]. Additionally, the NMR spectrum of  $\text{Li}_2\text{CO}_3$  reveals the solely tetrahedrally coordinated lithium in this compound (Figure 10c). A single shift of  $1.16$  ppm is observed, which is also in accordance to literature [28]. Since pristine compounds of  $\beta\text{-Li}_2\text{TiO}_3$  and spinel  $\text{Li}_4\text{Ti}_5\text{O}_{12}$  were yielded by solid state reactions, no  $\text{Li}_2\text{CO}_3$  may be present (confirmed by PXRD measurements). The third signal of  $\beta\text{-Li}_2\text{TiO}_3$  is therefore assigned to lithium on an interstitial position with tetrahedral coordination.

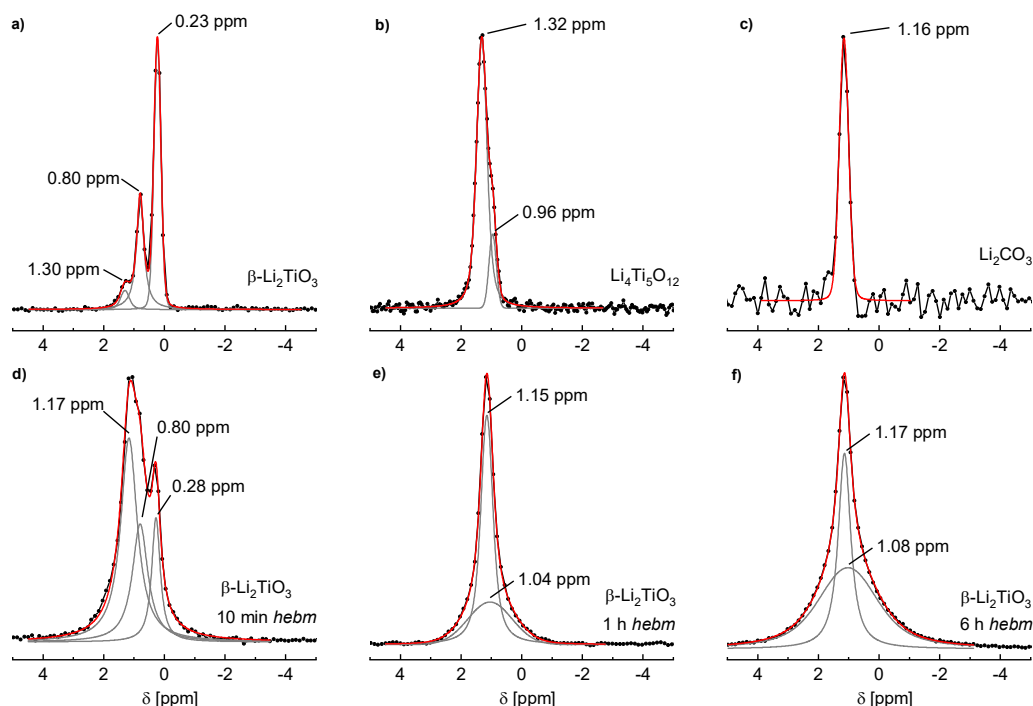


**Figure 10:**  $^6\text{Li}$  SPE MAS NMR spectra of a)  $\beta\text{-Li}_2\text{TiO}_3$ , b) spinel  $\text{Li}_4\text{Ti}_5\text{O}_{12}$ , c)  $\text{Li}_2\text{CO}_3$ , d)  $\beta\text{-Li}_2\text{TiO}_3$  after *hebm* for 10 min, e) 1 h and f) 6 h. All spectra were referenced against solid LiCl and fitted with one, two or three independent Voigt functions with  $R^2 > 0.99$ .

The spectrum of  $\beta\text{-Li}_2\text{TiO}_3$  after 10 min of milling is shown in Figure 10d. The signal at  $\delta = 1.30$  ppm is shifted to  $1.17$  ppm, while the two other shifts are hardly affected. Additionally, the signal intensities of  $\beta\text{-Li}_2\text{TiO}_3$  are strongly altered. The signal at  $1.17$  ppm indicates that more than half the lithium atoms are tetrahedrally coordinated, while only few remain in octahedral coordination. After 1 h of milling (Figure 10e) only two signals are present. The tetrahedral coordination remains as the dominant state with an additional new coordination environment indicated by a broad shift at  $1.04$  ppm. This situation is attributed to cubic  $\text{Li}_2\text{TiO}_3$  with Li and Ti in

octahedral coordination and a random ordering, causing this broadening. The signal at 1.15 ppm may be caused by  $\text{Li}_2\text{CO}_3$  that is formed after the milling process. However, PXRD refinements show a portion of only 19%  $\text{Li}_2\text{CO}_3$  after milling for 1 h, while the NMR signal is clearly caused by the main fraction in the sample. The tetrahedral coordination in  $\text{Li}_2\text{TiO}_3$  is therefore assumed to be a transition state for the formation of the cubic state. The new signal at ca. 1 ppm becomes the dominant state after milling for 6 h (Figure 10f). The  $^6\text{Li}$  SPE MAS NMR spectrum of  $\text{Li}_2\text{TiO}_3$  from milling of  $\text{LiOH}$  and rutile (WC tools, 6 h milling time) is nearly identical (not shown). This underlines the assumption that this broad signal is caused by octahedrally coordinated Li in the cubic phase. Parts of the tetrahedra signal remain. This is most probably caused by occupation of interstitial positions and by  $\text{Li}_2\text{CO}_3$ , but it was not possible to separate the contributions of these two states.

The  $^6\text{Li}$  SPE MAS NMR spectra of  $\text{Li}_4\text{Ti}_5\text{O}_{12}$  (supporting information, Figure SI8) show a slightly different behavior compared to the transformation of  $\beta\text{-Li}_2\text{TiO}_3$ . A broad signal at  $\delta = 1.15$  ppm is visible after milling for 1 h, indicating a purely tetrahedral coordination environment. No signal of an octahedral coordination at ca. 1 ppm is visible. Additionally, a small signal at 1.57 ppm can be distinguished. This signal indicates a very short Li-O bonding distance or a coordination number lower than four. This signal may either be attributed to an interstitial position or the unidentified phase seen in PXRD, but no further identification was possible.

In conclusion to the finding, that a tetrahedral coordination environment plays a major role in the structure after mechanochemical treatment, a revised structure model for the Rietveld refinement of  $\alpha\text{-Li}_2\text{TiO}_3$  was constructed. In the ideal NaCl structure model the octahedral 4a site is occupied by 1/3 Ti and 2/3 Li (model A). In the revised model, the tetrahedral 8c site was added and the corresponding site occupancy factors (*sof*) of Li on the 4a site (Li\_O) and 8c site (Li\_T) were refined. To keep the overall stoichiometry of  $\text{Li}_2\text{TiO}_3$ , a constraint refinement in the form [*sof*(Li\_T) =  $\frac{1}{3} - \frac{1}{2} \cdot \text{sof}(\text{Li}_\text{O})$ ] was defined, while the occupation of Ti was kept constant (model B). The resulting structure parameters are shown in Table 1.

**Table 1:** Structure model for the Rietveld refinement of  $\alpha\text{-Li}_2\text{TiO}_3$  with a mixed Li occupation in octahedral and tetrahedral gaps. Li\_T = tetrahedra gap, Li\_O = octahedra gap, WP = Wyckoff position, *sof* = site occupancy factor.

| site | WP | x   | y   | z   | atom             | sof     |
|------|----|-----|-----|-----|------------------|---------|
| Li_T | 8c | 1/4 | 1/4 | 1/4 | Li <sup>+</sup>  | 0.07(1) |
| Li_O | 4a | 0   | 0   | 0   | Li <sup>+</sup>  | 0.53(1) |
|      | 4a |     |     |     | Ti <sup>4+</sup> | 0.333   |
| O1   | 4b | 1/2 | 1/2 | 1/2 | O <sup>2-</sup>  | 1       |

In consequence of this adapted model, the Rietveld refinement of milled  $\beta\text{-Li}_2\text{TiO}_3$  (WC tools, 600 rpm, 6h) is improved. This can be seen particularly in the description of the 022 reflection, which is depicted in Figure 11 with a fit using the a) standard model A and b) the adjusted model B. To better accommodate the shape of the amorphous background, a polynomial of 25<sup>th</sup> degree was used in these both cases, instead of the otherwise used polynomial of 15<sup>th</sup> degree. Both the  $R_{\text{Bragg}}$  value of the  $\text{Li}_2\text{TiO}_3$  phase and the overall fit are improved in model B. The *GOF* is reduced from 1.13 in model A to 1.11 in model B, which is only slightly better but still indicating an improvement. Beyond that the  $R_{\text{Bragg}}$  value, which only depends on the agreement between observed and calculated reflection intensities of the phase, is significantly lowered from 0.60% in model A to 0.28% in model B. However, since Li has a very low X-ray scattering factor the obtained values for the site occupancies in Table 1 are just an indication of an occupation of the tetrahedral site and cannot be regarded as proof. Nevertheless, this model helps to harmonize the results of the Rietveld refinement with the fitted areas of the signals of tetrahedral and octahedral environments in the  $^6\text{Li}$  SPE MAS NMR spectrum of milled  $\beta\text{-Li}_2\text{TiO}_3$  (WC tools, 600 rpm, 6h). The areas in the  $^6\text{Li}$  spectrum sum up to a proportion of 0.59 to 1 for tetrahedral and octahedral coordinated lithium, which corresponds to 37% tetrahedrally coordinated lithium. The phase fraction from Rietveld refinement with model A (7%  $\text{Li}_2\text{CO}_3$ , 90%  $\alpha\text{-Li}_2\text{TiO}_3$  or 10.2 mol%  $\text{Li}_2\text{CO}_3$  and 88.3 mol%  $\alpha\text{-Li}_2\text{TiO}_3$ ) corresponds to only 10% tetrahedrally

coordinated lithium, solely arising from  $\text{Li}_2\text{CO}_3$ . This is far below the 37% from the  $^6\text{Li}$  spectrum. If tetrahedrally coordinated lithium in  $\alpha\text{-Li}_2\text{TiO}_3$  from model B (6.2%  $\text{Li}_2\text{CO}_3$ , 91.1%  $\alpha\text{-Li}_2\text{TiO}_3$  or 9.0 mol%  $\text{Li}_2\text{CO}_3$  and 89.5 mol%  $\alpha\text{-Li}_2\text{TiO}_3$ ) is factored in, a portion of 30% tetrahedrally coordinated lithium is obtained, which fits the portion of the Li NMR spectrum. Here, a *sof* of 0.07 for Li on the 8c site ( $\text{Li}_\text{T}$ ) correspond to 21% of tetrahedrally coordinated lithium in  $\alpha\text{-Li}_2\text{TiO}_3$ .

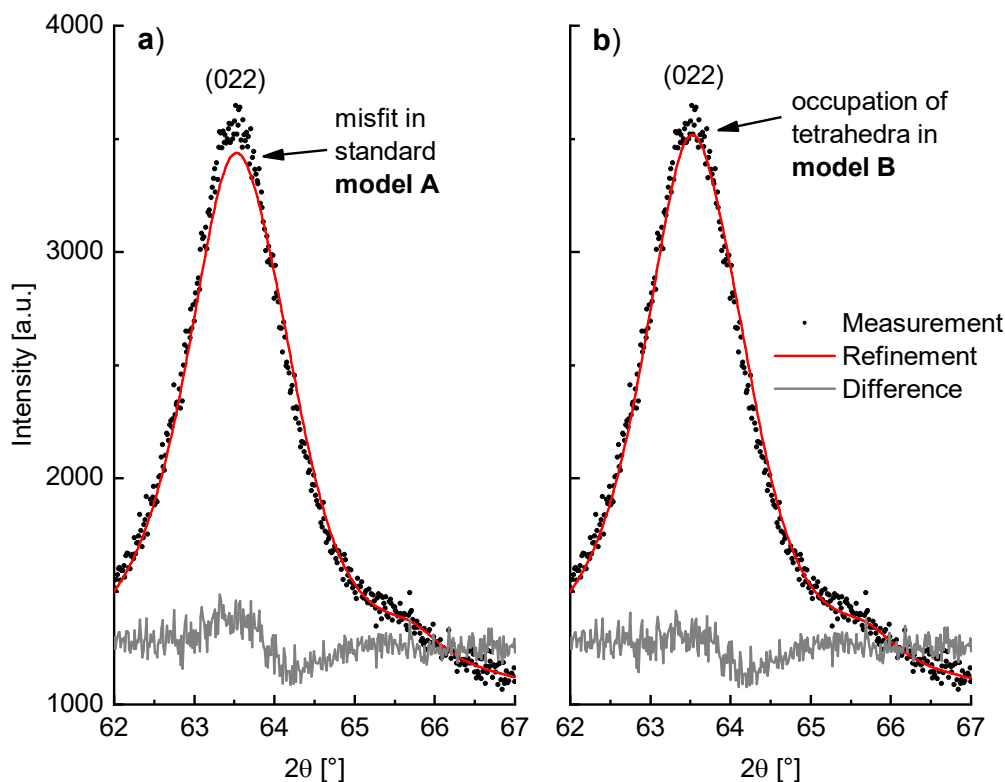


**Figure 11:** Rietveld refinement of milled  $\beta\text{-Li}_2\text{TiO}_3$  (WC tools, 600 rpm, 6h) with a) the ideal NaCl structure model and b) a NaCl structure with mixed Li occupation in octahedra and tetrahedra gaps. Refinement parameters: a)  $R_{\text{Bragg}} = 0.60\%$ ,  $\text{GOF} = 1.13$  and b)  $R_{\text{Bragg}} = 0.28\%$ ,  $\text{GOF} = 1.11$ .

### 2.5 Impedance spectroscopy

Since ball milling leads to the formation of defects, structure deformations and amorphization, an influence on the ion conductivity can be expected. The impedance spectra of ball milled  $\text{Li}_2\text{TiO}_3$  (600 rpm) and  $\text{Li}_4\text{Ti}_5\text{O}_{12}$  (400 rpm) show an increase in conductivity of up to three orders of magnitude. The frequency dependent real part of the conductivity is shown in Figure 12a and b. The spectra were recorded at 298K.

The conductivity of  $\text{Li}_2\text{TiO}_3$  from the solid-state reaction is rather poor and is immeasurable at frequencies below 3 kHz. After milling for 10 min an increase of one order of magnitude can be observed, with a typical dc plateau ( $\sigma_{\text{dc}} \approx 10^{-6}$  S/cm) at lower frequencies and a dispersive regime at higher frequencies. Similar results are shown by Brandstätter et al. [16], however, only a conductivity  $\sigma_{\text{dc}}$  of about  $10^{-9}$  S/cm is reported at room temperature for a milled sample. Milling of  $\text{Li}_2\text{TiO}_3$  for 1 h decreases the conductivity to  $\approx 10^{-7}$  S/cm, indicating a blocking of the Li ion transport. This may be due to the phase transformation from  $\beta$ - to  $\alpha\text{-Li}_2\text{TiO}_3$ . As already shown by  $^6\text{Li}$  MAS NMR in Figure 10, milling for 10 min displaces Li to tetrahedrally coordinated sites, which may be responsible for the increase in conductivity. Longer milling times promote a new octahedral coordinated state, that may be associated to the decrease in conductivity.

$\text{Li}_4\text{Ti}_5\text{O}_{12}$  shows a similar behavior to  $\text{Li}_2\text{TiO}_3$ , with a dc plateau at lower and a dispersive region at higher frequencies and a decrease of the conductivity after longer milling times. However,  $\text{Li}_4\text{Ti}_5\text{O}_{12}$  from solid state reaction already exhibits a dc plateau at lower frequencies with  $\sigma_{\text{dc}} \approx 10^{-7}$  S/cm at

298K. Milling for 10 min increases the conductivity by three orders of magnitude to  $>10^{-4}$  S/cm at 298K. The observed conductivities are the highest shown yet for ball milled  $\text{Li}_4\text{Ti}_5\text{O}_{12}$  at room temperature [18].

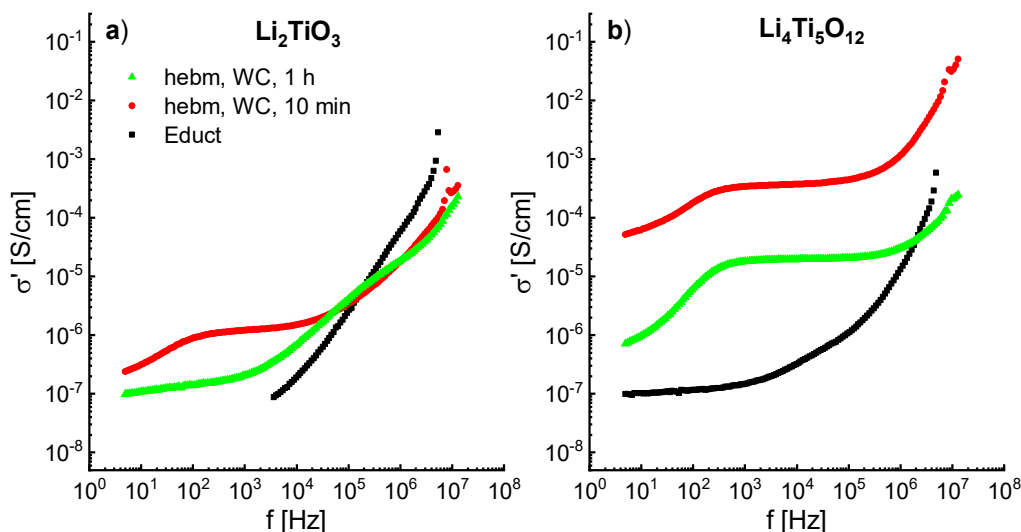


**Figure 12:** Frequency dependent real part of the conductivity at 298K of a)  $\text{Li}_2\text{TiO}_3$  and b)  $\text{Li}_4\text{Ti}_5\text{O}_{12}$  before and after milling at a) 600 rpm and b) 400 rpm for 10 min and 1 h.

### 3. Materials and Methods

#### 3.1 Materials

$\text{LiOH}$  (Merck, 98%),  $\text{Li}_2\text{CO}_3$  (Merck, 99%),  $\text{TiO}_2$  (Anatase, Merck,  $\geq 99\%$  and Rutile, Alfa Aesar, 99.5%), 2-propanole (Biesterfeld Spezialchemie, 97%) and *n*-pentane (Sigma Aldrich, 99%) were used as received. All solids have been characterized by PXRD. The used  $\text{LiOH}$  contained 20%  $\text{LiOH}\cdot\text{H}_2\text{O}$ .

#### 3.2 Sample Preparation

Milling was conducted in a Retsch PM100 planetary ball mill with rotational speeds of 400, 500 and 600 rpm. Milling tools consisting of yttrium stabilized zirconia ( $\text{ZrO}_2$ ) and tungsten carbide in cobalt matrix (WC) with a volume of 50 mL as well as 200 milling balls of the same material, with a diameter of 5 mm were used. The ball to powder weight ratio was 27:1 in case of  $\text{ZrO}_2$  and 60:1 in case of WC tools. Approximately 3 g of starting powder ( $\text{Li}_4\text{Ti}_5\text{O}_{12}$  or  $\beta\text{-Li}_2\text{TiO}_3$ ) were placed in the grinding jar. To prevent cementing of the powders, 200  $\mu\text{L}$  of 2-propanole were added as dispersing agent. In case of the mechanochemical synthesis from binary oxides,  $\text{LiOH}$  and  $\text{TiO}_2$  (rutile or anatase) to form 3 g of  $\text{Li}_2\text{TiO}_3$  were deployed. An excess of 10 mol%  $\text{LiOH}$  was used.

Spinel  $\text{Li}_4\text{Ti}_5\text{O}_{12}$  and  $\beta\text{-Li}_2\text{TiO}_3$  were synthesized by conventional solid-state reactions [6,29]. Appropriate amounts of lithium carbonate and anatase were homogenized by wet ball milling with *n*-pentane at 400 rpm for 1 h. A 50 mL agate grinding jar and twenty agate balls of 10 mm diameter were used. The dried mixtures were heated in a platinum crucible to 900  $^\circ\text{C}$  for 8 h in air atmosphere. The resulting white powders were manually ground in an agate mortar and reheated a second time. To obtain samples of  $\beta\text{-Li}_2\text{TiO}_3$  with higher crystallinity and less Li-Ti-disorder, several heating steps at 1100  $^\circ\text{C}$  were carried out.

#### 3.3 Characterization

Powder X-ray diffraction (PXRD) patterns were recorded on a Bruker D8-A25-Advance diffractometer in Bragg-Brentano  $\theta$ - $\theta$ -geometry (goniometer radius 280 mm) with  $\text{CuK}\alpha$ -radiation ( $\lambda = 154.0596$  pm). A 12  $\mu\text{m}$  Ni foil working as  $\text{K}\beta$  filter and a variable divergence slit were mounted



at the primary beam side. A LYNXEYE detector with 192 channels was used at the secondary beam side. Experiments were carried out in a  $2\theta$  range of 7 to  $120^\circ$  with a step size of  $0.013^\circ$  and a total scan time of 2 h. Topas 4.2 [30] was used for the Rietveld refinements. Crystallographic structure and microstructure were refined, while instrumental line broadening was included in a fundamental parameters approach [31]. The background was fitted by a Chebychev polynomial function of 15<sup>th</sup> degree, while fluorescence induced background was reduced by discriminating the detector. Crystal structure data were obtained from the crystallography open database (COD) [32] and inorganic crystal structure database (ICSD).

Thermogravimetric analysis was conducted on a Netzsch TG 209 F1 Iris ASC in alumina crucibles ( $V = 75 \mu\text{L}$ ), in a temperature range from 25 – 1000 °C under a nitrogen flow of  $40 \text{ mL}\cdot\text{min}^{-1}$  with a heating rate of  $20 \text{ K}\cdot\text{min}^{-1}$ . The samples were dried in a pre-heating phase at 100 °C under flowing nitrogen and cooled again before the measurement was started. Coupling of the gas flow to a Bruker Vertex 70 IR spectrometer was achieved with a heated transfer line (200 °C) under constant nitrogen flow. Spectra were recorded between 4500 to  $600 \text{ cm}^{-1}$  with a resolution of  $4 \text{ cm}^{-1}$  and 32 scans per spectrum.

$^6\text{Li}$  single-pulse excitation magic angle spinning (SPE MAS) NMR spectra were recorded on a Bruker AV400WB spectrometer ( $^6\text{Li}$  at 58.91 MHz) at 298K in standard  $\text{ZrO}_2$  rotors ( $d = 4 \text{ mm}$ ). A spinning rate of 12 to 13 kHz and a relaxation delay of 3 s were used. Solid LiCl was used as external reference at 0 ppm.

Impedance spectra were recorded on an HP 4192A impedance analyzer in a frequency range of 5 Hz to 13 MHz at 298K. Data points were recorded via software [33]. The samples were pressed into pellets with 10 mm diameter and a thickness of 1.4 – 2.1 mm under a uniaxial pressure of 250 MPa at room temperature. Both sides of the pellets were coated with silver conducting paste and dried overnight in air, to establish electrical contact with the platinum electrodes in the measurement cell.

### 3.4 Structural model for $\beta\text{-Li}_2\text{TiO}_3$ in Rietveld refinement

As already mentioned in literature, Rietveld refinement of  $\beta\text{-Li}_2\text{TiO}_3$  requires a more complex structural model than a single well-ordered phase. A mixed occupancy of Li and Ti in the  $\text{LiTi}_2$  layer and different stacking variants must be considered to obtain a satisfactory fit [34]. In our work a three-fraction model [35,36] with a Li-Ti-mixing in the  $\text{LiTi}_2$  layer was used to account for a distribution of different states, but no stacking variants were considered. The parameters of the microstructure of the three fractions were constrained but lattice parameters were refined independently.

## 4. Conclusions

The cubic polymorph of  $\text{Li}_2\text{TiO}_3$  was successfully synthesized via high energy ball milling of LiOH with rutile,  $\beta\text{-Li}_2\text{TiO}_3$  and spinel  $\text{Li}_4\text{Ti}_5\text{O}_{12}$ . The material of the used milling tools showed a large impact on the composition of the product powders. Use of tungsten carbide (WC) led to full conversion of rutile with LiOH or  $\beta\text{-Li}_2\text{TiO}_3$  to  $\alpha\text{-Li}_2\text{TiO}_3$ . In contrast, the use of yttrium stabilized zirconia ( $\text{ZrO}_2$ ) did not lead to full conversion, neither of rutile with LiOH nor  $\beta\text{-Li}_2\text{TiO}_3$  regardless of the applied milling conditions. TG-IR coupling of the gas flow showed primarily characteristic bands of  $\text{CO}_2$ , indicating crystalline  $\text{Li}_2\text{CO}_3$  to be mainly responsible for the mass loss upon heating. Therefore, the amorphous background is assumed to primarily consist of  $\text{TiO}_2$ .

Heating under mild conditions (200 °C for 1 h) of the mechanically produced cubic phase caused a phase percentage of 90% cubic phase, without affecting the nano-crystallinity. Further heating resulted in an ordering phenomenon with monoclinic structure at lower temperatures, following a discrete structure change between 600 and 700 °C resulting in a full transformation to  $\beta\text{-Li}_2\text{TiO}_3$ .

Even after mild milling conditions, the structure of spinel  $\text{Li}_4\text{Ti}_5\text{O}_{12}$  is strongly altered, which may have large impact on the use of mechanochemical treated  $\text{Li}_4\text{Ti}_5\text{O}_{12}$  as anode material. Though a phase with cubic structure was formed, the reflections were very broad and additional unidentified reflections were visible.

$^6\text{Li}$  SPE MAS NMR spectra revealed an extensive rearrangement of the Li environment in  $\beta\text{-Li}_2\text{TiO}_3$  after 10 min of milling. A tetrahedrally coordinated state may be occupied by Li. NMR

spectra of the mechanochemically treated spinel  $\text{Li}_4\text{Ti}_5\text{O}_{12}$  indicated a purely tetrahedrally coordinated environment after milling for 1 h. The process of the milling induced transformation of the spinel is not completely understood yet. In conclusion to these findings, a revised structure model including a tetrahedral Li site in cubic  $\text{Li}_2\text{TiO}_3$  was tested in Rietveld refinement and resulted in a slightly improved fit.

Impedance spectroscopy measurements at 298K show an increase in conductivity of up to three orders of magnitude after milling for just 10 min. This may be due to the displacement of Li ions to tetrahedrally coordinated or interstitial sites (as observed by  $^6\text{Li}$  NMR). Longer milling times tend to decrease the conductivity again. These results may be a hint how to activate anode materials for a faster lithium intercalation.

**Supplementary Materials:** The following are available online at [www.mdpi.com/link](http://www.mdpi.com/link), Figure S1: Rietveld refinement of the milling product from LiOH and anatase, Figure S2: Rietveld refinement of the milling product from LiOH and rutile, Figure S3: SEM photograph of the milling product from LiOH and rutile, Table S11: Refined structure parameters of  $\alpha$ - $\text{Li}_2\text{TiO}_3$  produced by milling of LiOH and rutile, Figure S14: TGA and calculated DTA curve of  $\text{Li}_2\text{TiO}_3$  from milling of LiOH and rutile, Figure S15: Temperature dependent IR signals from coupling of TGA gas flow to IR detector, Figure S16: Rietveld refinement of the milling product from LiOH and rutile, Figure S17: Rietveld refinement of  $\beta$ - $\text{Li}_2\text{TiO}_3$  after ball milling with WC tools for 6 h at 600 rpm, Figure S18:  $^6\text{Li}$  SPE MAS NMR spectra of a) spinel  $\text{Li}_4\text{Ti}_5\text{O}_{12}$ , b) after *hebm* for 1 h.

**Acknowledgments:** We would like to thank Christina Odenwald for recording of the SEM photographs and Michael Zimmer for conducting the NMR experiments and helpful discussion.

**Author Contributions:** Conceptualization, D.B., R.H. and G.K.; Methodology and Formal Analysis, D.B. and R.H.; Investigation, D.B.; Resources, G.K.; Writing – Original Draft Preparation, D.B.; Writing – Review & Editing, D.B., R.H., and G.K.; Visualization, D.B.; Supervision, R.H. and G.K.

**Conflicts of Interest:** The authors declare no conflict of interest.

## References

1. Fuentes, A. F.; Takacs, L. Preparation of Multicomponent Oxides by Mechanochemical Methods. *J. Mater. Sci.* **2013**, *48* (2), 598–611, 10.1007/s10853-012-6909-x.
2. Chaudhuri, J.; Ram, M. L.; Sarkar, B. K. Observation of a High Pressure Polymorph of Titania by Vibrational Ball Milling. *J. Mater. Sci.* **1994**, *29* (13), 3484–3488, 10.1007/BF00352053.
3. Kong, L.; Ma, J.; Zhu, W.; Tan, O. Phase Formation and Thermal Stability of  $(\text{Zr}_{1-x}\text{Ti}_x)\text{O}_2$  Solid Solution via a High-Energy Ball Milling Process. *J. Alloys Compd.* **2002**, *335* (1–2), 290–296, 10.1016/S0925-8388(01)01844-8.
4. Fischer, A.; Ney, C.; Kickelbick, G. Synthesis of Surface-Functionalized Titania Particles with Organophosphorus Coupling Agents by Reactive Milling. *Eur. J. Inorg. Chem.* **2013**, *2013* (33), 5701–5707, 10.1002/ejic.201300589.
5. Amade, R.; Heitjans, P.; Indris, S.; Finger, M.; Haeger, A.; Hesse, D. Defect Formation during High-Energy Ball Milling in  $\text{TiO}_2$  and Its Relation to the Photocatalytic Activity. *J. Photochem. Photobiol. A Chem.* **2009**, *207* (2–3), 231–235, 10.1016/j.jphotochem.2009.07.015.
6. Lang, G. Die Kristallstruktur Einiger Vertreter Der Verbindungsklasse  $\text{Me}_2\text{Me}^{\text{IV}}\text{O}_3$  Als Beitrag Zur Aufklärung Der Ordnungsphase von  $\text{Li}_2\text{TiO}_3$ . *ZAAC, J. Inorg. Gen. Chem.* **1954**, *276* (1–2), 77–94, 10.1002/zaac.19542760109.
7. Giquel, C.; Mayer, M. M.; Bouaziz, R.; Champetier, M. G. Sur Quelques Composés Oxygénés Du Titane et Des Alcalins (Li, Na); Étude Des Binaires  $\text{M}_2\text{O-TiO}_2$  Dans Les Zones Riches En Oxyde Alcalin. *C. R. Acad. Sc. Paris* **1972**, *275* (C), 1427–1430.
8. Mikkelsen, J. C. Pseudobinary Phase Relations of  $\text{Li}_2\text{Ti}_3\text{O}_7$ . *J. Am. Ceram. Soc.* **1980**, *63* (5–6), 331–335, 10.1111/j.1151-2916.1980.tb10732.x.
9. Kleykamp, H. Phase Equilibria in the Li–Ti–O System and Physical Properties of  $\text{Li}_2\text{TiO}_3$ . *Fusion Eng. Des.* **2002**, *61–62*, 361–366, 10.1016/S0920-3796(02)00120-5.
10. Kleykamp, H. Enthalpy, Heat Capacity and Enthalpy of Transformation of  $\text{Li}_2\text{TiO}_3$ . *J. Nucl. Mater.* **2001**, *295* (2–3), 244–248, 10.1016/S0022-3115(01)00550-5.

11. Tomiha, M.; Masaki, N.; Uchida, S.; Sato, T. Hydrothermal Synthesis of Alkali Titanates from Nano Size Titania Powder. *J. Mater. Sci.* **2002**, *37* (11), 2341–2344, 10.1023/A:1015337824541.
12. Song, H.; Jiang, H.; Liu, T.; Liu, X.; Meng, G. Preparation and Photocatalytic Activity of Alkali Titanate Nano Materials  $A_2Ti_nO_{2n+1}$  ( $A=Li, Na$  and  $K$ ). *Mater. Res. Bull.* **2007**, *42* (2), 334–344, 10.1016/j.materresbull.2006.05.025.
13. Laumann, A.; Fehr, K. T.; Wachsmann, M.; Holzapfel, M.; Iversen, B. B. Metastable Formation of Low Temperature Cubic  $Li_2TiO_3$  under Hydrothermal Conditions — Its Stability and Structural Properties. *Solid State Ionics* **2010**, *181* (33–34), 1525–1529, 10.1016/j.ssi.2010.08.017.
14. Laumann, A.; Ørnsbjerg Jensen, K. M.; Tyrsted, C.; Bremholm, M.; Fehr, K. T.; Holzapfel, M.; Iversen, B. B. In-Situ Synchrotron X-Ray Diffraction Study of the Formation of Cubic  $Li_2TiO_3$  Under Hydrothermal Conditions. *Eur. J. Inorg. Chem.* **2011**, *2011* (14), 2221–2226, 10.1002/ejic.201001133.
15. Laumann, A.; Fehr, K. T.; Boysen, H.; Hölzel, M.; Holzapfel, M. Temperature-Dependent Structural Transformations of Hydrothermally Synthesized Cubic  $Li_2TiO_3$  Studied by in-Situ Neutron Diffraction. *Zeitschrift für Krist.* **2011**, *226* (1), 53–61, 10.1524/zkri.2011.1286.
16. Brandstätter, H.; Wohlmuth, D.; Bottke, P.; Pregartner, V.; Wilkening, M. Li Ion Dynamics in Nanocrystalline and Structurally Disordered  $Li_2TiO_3$ . *Z. Phys. Chem.* **2015**, *229* (9), 1363–1374, 10.1515/zpch-2014-0665.
17. Carbajal-Ramos, I. A.; Andrade-Gamboa, J. J.; Condó, A. M.; Gennari, F. C. Formation of Cubic  $Li_2TiO_3$  by Mechanical Activation and Its Transformation to Monoclinic Phase: Stability in Helium and Hydrogen Flows. *Solid State Ionics* **2017**, *308*, 46–53, 10.1016/j.ssi.2017.05.017.
18. Iwaniak, W.; Fritzsche, J.; Zukalová, M.; Winter, R.; Wilkening, M.; Heitjans, P. Li Conductivity of Nanocrystalline  $Li_4Ti_5O_{12}$  Prepared by a Sol-Gel Method and High-Energy Ball Milling. *Defect Diffus. Forum* **2009**, *289–292*, 565–570, 10.4028/www.scientific.net/DDF.289-292.565.
19. Becker, D.; Haberkorn, R.; Kickelbick, G. Mechanochemical Synthesis of Cubic  $Li_2TiO_3$ . *Zeitschrift für Krist. - Suppl.* **2017**, *37*, P178.
20. Indris, S.; Amade, R.; Heitjans, P.; Finger, M.; Haeger, A.; Hesse, D.; Grünert, W.; Börger, A.; Becker, K. D. Preparation by High-Energy Milling, Characterization, and Catalytic Properties of Nanocrystalline  $TiO_2$ . *J. Phys. Chem. B* **2005**, *109* (49), 23274–23278, 10.1021/jp054586t.
21. Obrovac, M. Structure and Electrochemistry of  $LiMO_2$  ( $M=Ti, Mn, Fe, Co, Ni$ ) Prepared by Mechanochemical Synthesis. *Solid State Ionics* **1998**, *112* (1–2), 9–19, 10.1016/S0167-2738(98)00225-2.
22. Jiang, K.; Hu; Sun; Wang; Jin; Ren; Chen, G. Z. Electrochemical Synthesis of  $LiTiO_2$  and  $LiTi_2O_4$  in Molten  $LiCl$ . *Chem. Mater.* **2004**, *16* (22), 4324–4329, 10.1021/cm0494148.
23. Betke, A.; Kickelbick, G. Important Reaction Parameters in the Synthesis of Phenylphosphonic Acid Functionalized Titania Particles by Reactive Milling. *New J. Chem.* **2014**, *38* (3), 1264–1270, 10.1039/C3NJ01291C.
24. Gajovic, A.; Furic, K.; Music, S.; Djerdj, I.; Tonejc, A.; Tonejc, A. M.; Su, D.; Schlogl, R. Mechanism of  $ZrTiO_4$  Synthesis by Mechanochemical Processing of  $TiO_2$  and  $ZrO_2$ . *J. Am. Ceram. Soc.* **2006**, *89* (7), 2196–2205, 10.1111/j.1551-2916.2006.00972.x.
25. Vijayakumar, M.; Kerisit, S.; Yang, Z.; Graff, G. L.; Liu, J.; Sears, J. A.; Burton, S. D.; Rosso, K. M.; Hu, J. Combined  $^6Li$  NMR and Molecular Dynamics Study of Li Diffusion in  $Li_2TiO_3$ . *J. Phys. Chem. C* **2009**, *113* (46), 20108–20116, 10.1021/jp9072125.
26. Baklanova, Y. V.; Arapova, I. Y.; Shein, I. R.; Maksimova, L. G.; Mikhalev, K. N.; Denisova, T. A. Charge Distribution and Mobility of Lithium Ions in  $Li_2TiO_3$  from  $^6Li$  NMR Data. *J. Struct. Chem.* **2013**, *54* (S1), 111–118, 10.1134/S002247661307010X.
27. Xu, Z.; Stebbins, J. F.  $^6Li$  Nuclear Magnetic Resonance Chemical Shifts, Coordination Number and Relaxation in Crystalline and Glassy Silicates. *Solid State Nucl. Magn. Reson.* **1995**, *5* (1), 103–112, 10.1016/0926-2040(95)00026-M.
28. Kartha, J. P.; Tunstall, D. P.; Irvine, J. T. S. An NMR Investigation of Lithium Occupancy of Different Sites in the Oxide Superconductor  $LiTi_2O_4$  and Related Compounds. *J. Solid State Chem.* **2000**, *152* (2), 397–402, 10.1006/jssc.2000.8696.
29. Leonidov, I. A.; Leonidova, O. N.; Perelyaeva, L. A.; Samigullina, R. F.; Kovyazina, S. A.; Patrakeev, M. V. Structure, Ionic Conduction, and Phase Transformations in Lithium Titanate  $Li_4Ti_5O_{12}$ . *Phys. Solid State* **2003**, *45* (11), 2183–2188, 10.1134/1.1626760.
30. Topas 4.2. General Profile and Structure Analysis Software for Powder Diffraction Data. *Bruker AXS, Karlsruhe, Germany* **2009**.

- 
31. Cheary, R. W.; Coelho, A. A.; Cline, J. P. Fundamental Parameters Line Profile Fitting in Laboratory Diffractometers. *J. Res. Natl. Inst. Stand. Technol.* **2004**, *109* (1), 1–25, 10.6028/jres.002.
  32. Gražulis, S.; Chateigner, D.; Downs, R. T.; Yokochi, A. F. T.; Quirós, M.; Lutterotti, L.; Manakova, E.; Butkus, J.; Moeck, P.; Le Bail, A. Crystallography Open Database – an Open-Access Collection of Crystal Structures. *J. Appl. Crystallogr.* **2009**, *42* (4), 726–729, 10.1107/S0021889809016690.
  33. Lücke, H. HPLueke Version 2 - A Program for Running an HP 4192A Impedance Analyzer. **2016**.
  34. Tarakina, N. V.; Neder, R. B.; Denisova, T. A.; Maksimova, L. G.; Baklanova, Y. V.; Tyutyunnik, A. P.; Zubkov, V. G. Defect Crystal Structure of New  $\text{TiO}(\text{OH})_2$  Hydroxide and Related Lithium Salt  $\text{Li}_2\text{TiO}_3$ . *Dalton Trans.* **2010**, *39* (35), 8168, 10.1039/c0dt00354a.
  35. Beck, H. P.; Douiheche, M.; Haberkorn, R.; Kohlmann, H. Synthesis and Characterisation of Chloro-Vanadato-Apatites  $M_5(\text{VO}_4)_3\text{Cl}$  ( $M = \text{Ca}, \text{Sr}, \text{Ba}$ ). *Solid State Sci.* **2006**, *8* (1), 64–70, 10.1016/j.solidstatesciences.2005.08.014.
  36. Haberkorn, R.; Bauer, J.; Kickelbick, G. Chemical Sodiation of  $\text{V}_2\text{O}_5$  by  $\text{Na}_2\text{S}$ . *Z. Anorg. Allg. Chem.* **2014**, *640* (15), 3197–3202, 10.1002/zaac.201400381.